Electronic Supplementary Material (ESI) for Lab on a Chip.

Supplementary Information

Tetra-primer ARMS-PCR combined with dual-color fluorescent lateral flow assay for the discrimination of SARS-CoV-2 and its mutations with a handheld wireless reader

Yunxiang Wang[a,b,1], Hong Chen[a,b,1], Hongjuan Wei[a,b], Zhen Rong[a,b,*], Shengqi Wang[a,b,*]

[a]Beijing Institute of Radiation Medicine, Beijing 100850, P. R. China.

[b]Beijing Key Laboratory of New Molecular Diagnosis Technologies for Infectious Diseases, Beijing 100850, P. R. China.

[1]Y.-X. Wang and H. Chen contributed equally to this work.

Corresponding Author

*(S.-Q. Wang) E-mail: sqwang@bmi.ac.cn.

*(Z. Rong) E-mail: rongzhen0525@sina.com.

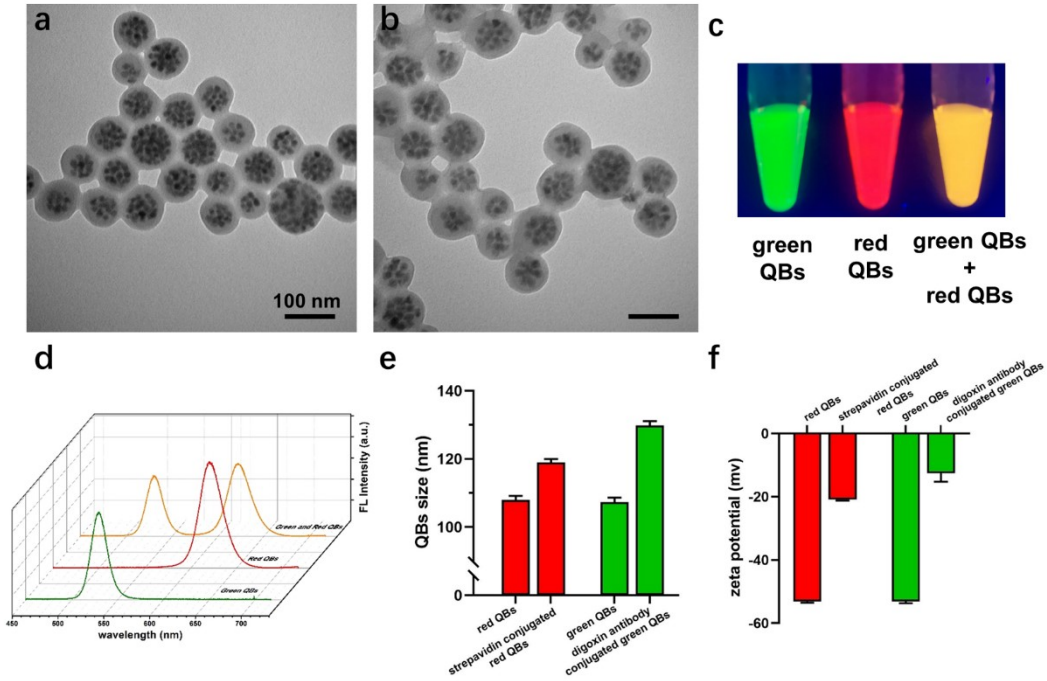

Fig. S1. Characterization of QBs. TEM images of (a) green QBs and (b) red QBs. (c) Images and (d) fluorescence spectra of green QBs, red QBs, and their mixture under the excitation of UV light. (e) DLS sizes and (f) zeta potentials of green and red QBs before and after conjugation of antibody or streptavidin. Error bars represent the standard deviation of three repetitive experiments.

Optimization of the primer concentration. In this work, the primer concentration was found as a key factor of the method. Higher primer concentration readily resulted in primer dimers that can be recognized by the capture and detection antibodies, thus leading to the appearance of false-positive signals on the test lines. Four different concentrations (50 nM, 30 nM, 15 nM and 10 nM) of the primers for D614G were tested to obtain the optimal primer concentration. As shown in Fig. S2, the 50 nM and 30 nM **primer** concentrations resulted in higher fluorescence intensity, but the results demonstrated the nonspecific signals. Both red and green channel signals were obvious and resulted in yellow color on the test line. Though the fluorescence intensity of 15 nM primer concentration is lower than 50 nM and 30 nM, but it presented an apparent specific signal. When the mutant RNA templates were added into reaction mixture, the fluorescence intensity of the red channel was evidently higher than the green channel. Instead, when the added sample was wild-type, the signal of the green channel was dominant. The 10 nM primer concentration led to a negative result. Therefore, the optimum primer concentration was 15 nM.

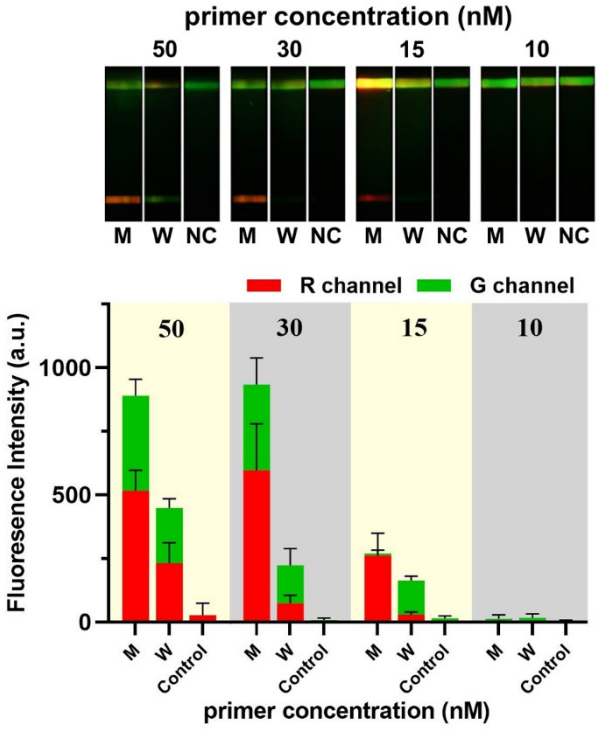

Fig. S2. The images and the fluorescence intensity of the test strips for the primer concentration of 50, 30, 15, and 10 nM. Error bars represent the standard deviation of three repetitive experiments.

Optimization of the ratio of inner primer to outer primer. In this reaction mixture, the RNA fragment between the two outer primers can be amplified regardless of its mutant status. Four different ratios of inner primer to out primer of 10:1, 5:1, 2:1 and 1:1 with constant 15 nM of out primer, were selected to evaluate its effect on assay performance. As shown in the Fig. S3, the ratio of 5:1 and 2:1 demonstrated a stronger red fluorescence signal, while the green fluorescence signal was weakly enhanced. Furthermore, a ratio of 10:1 exhibited a strong specific fluorescence intensity of both red channel and green channel on the test line, which was attributed to the increased amount of the two shorter allele-specific amplicons.

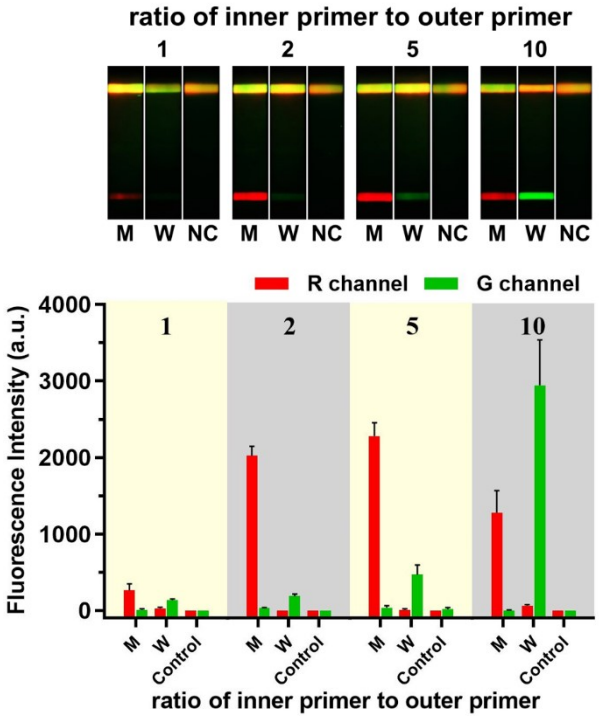

Fig. S3. The images and the fluorescence intensity of the test strips for the ratio of inner primer to outer primer of 1, 2, 5, and 10. Error bars represent the standard deviation of three repetitive experiments.

Optimization of the annealing temperature. The effect of different annealing temperatures (58 ℃, 60 ℃, 62 ℃ and 64 ℃) were investigated. As shown in the Fig. S4, the resulted test line of mutated sequence with the lower annealing temperature (58 ℃) was yellow colored as a result of the non-specific amplification. Meanwhile, higher annealing temperature (64 ℃) reduced the efficiency of the amplification. The optimal annealing temperature was determined as 62 ℃, which exhibited a significantly enhanced signal for both red and green channel without nonspecific products.

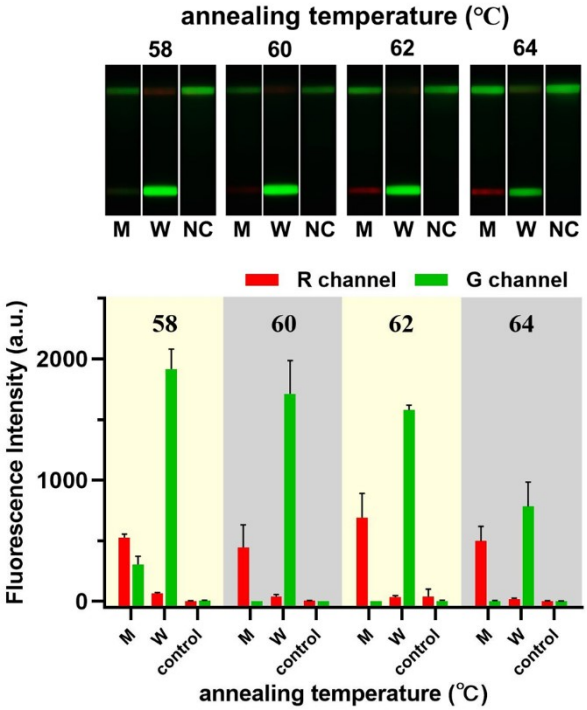

Fig. S4. The images and the fluorescence intensity of the test strips for annealing temperature of 58, 60, 62, and 64 ℃. Error bars represent the standard deviation of three repetitive experiments.

Fig. S5. Test strip images for influenza A virus (IAV), influenza B virus (IBV), and adenovirus (ADV).

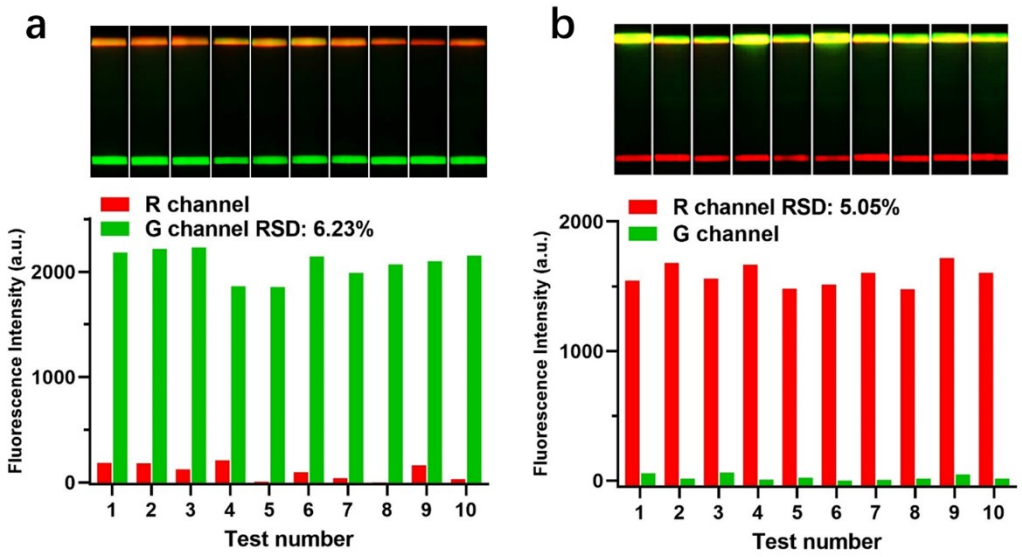

Fig. S6. Reproducibility of the test strips for 10^4 copies/μL of (a) 614D and (b) 614G.

Table S1. Primer sequences used for discrimination of N501Y and D614G of SARS-CoV-2 variants and simultaneous detection of N gene and ORF1ab gene of SARS-CoV-2.

Application	Name	Sequence (5' - 3')	5'-Modification	Product length
N501Y	501-M-F	CGGTAGCACACCTTGTAATGG	biotin	100bp
	501-M-R	GTATGGTTGGTAACCAACACCAAA	FITC	
	501-WT-F	TCATATGGTTTCCAACCCACAA	FITC	181bp
	501-WT-R	CAGTAAGAACACCTGTGCCTGT	digoxin	
D614G	614-M-F	ACAGACACTTGAGATTCTTGACAT	biotin	126bp
	614-M-R	GGGACTTCTGTGCAGTTAAAAC	TAMRA	
	614-WT-F	CAGGTTGCTGTTCTTTATCAGAA	TAMRA	184bp
	614-WT-R	CACCAATGGGTATGTCACACTCA	digoxin	
N gene	N-F	ATGGCGGTGATGCTGCTCTTG	biotin	209bp
	N-R	GGTTTGTTCTGGACCACGTCTGC	TAMRA	
ORF1ab gene	ORF-F	GTTGCCACATAGATCATCCAAATC	digoxin	157bp
	ORF-R	CAACTACAGCCATAACCTTTCCAC	TAMRA	

Table S2. Bill of materials for the handheld wireless reader.

Item	Manufacturer	Catalog	Quantity	Price ($)	Cost ($)
Stepper motor and screw	Dzyk Electrical & Mechanical Co., Ltd.	E20PA14A05-55-001	1	46.56	46.56
Stepper motor slide	CPC Corporation	MR7MN	1	11.56	11.56
Optical filter	Beijing Bodian Optical Tech Co., Ltd.	365/42 nm, mm diameter	1	4.69	4.69
		525/20 nm, 7mm diameter	1	16.56	16.56
		610/20 nm, 7mm diameter	1	16.56	16.56
UV LED	Shenzhen Chaoziran Tech Co., Ltd.	20mA	1	1.17	1.17
Photodiode	Hamamatsu Photonics Co., Ltd.	S2386-45K	2	8.44	16.88
Lithium battery	Shenzhen Wonzer Technology Co., Ltd.	805080, 4000mAh, 3.7V	1	2.53	2.53
Electronic components			1	7.81	7.81
Mechanical parts		Custom-made	1	15.62	15.62
3D-printed reader enclosure			1	6.25	6.25
Total					**146.19**

Table S3. The fluorescence intensity of M and W D614G in Figure 4.

	M D614G			***W D614G***		
concentration (copies/ul)	**R Channel**	**G Channel**	**R/G**	**R Channel**	**G Channel**	**G/R**
0	4.83	0.98	4.93	4.83	0.98	0.20
10	8.06	0.01	806.00	4.44	7.98	1.80
50	43.90	5.52	7.95	0.01	3.76	564.50
100	67.69	0.03	2256.22	0.20	1.63	8.00
500	660.75	0.01	49556.25	0.13	146.15	1153.84
1000	1327.93	39.33	33.77	4.52	168.73	37.33
5000	1529.25	25.74	59.42	2.71	888.16	327.73
10000	1622.63	52.08	31.15	31.93	2164.94	67.80
50000	1663.29	57.09	29.14	50.09	3611.69	72.11
100000	1699.27	33.61	50.56	47.82	3900.20	81.57

Table S4. Comparison of assay sensitivity for SARS-CoV-2 mutations.

Method	Limit of detection	Mutation site	Ref.
Real-time RT-PCR	117 copies/reaction	E484K N501Y	S1
Immunodetection	1×10^4 pfu/ml $2\text{-}3\times10^4$ pfu/ml	501Y.V1 variant 501Y.V2 variant	S2
CRISPR-Cas13-Based Transcription Amplification	82 copies/reaction	D614G	S3
CRISPR-based POC diagnostic platform	1100 copies/ml 1200 copies/ml 49000 copies/ml	Y144Del E484K N501Y	S4
CRISPR-Cas9-based LFA	Ct value=34	N501Y	S5
Tetra-primer ARMS-PCR based LFA	78.91 copies μL^{-1} 33.53 copies μL^{-1}	wild-type 614 mutant 614	this work

Reference

S1. Chaintoutis, S. C.; Chassalevris, T.; Tsiolas, G.; Balaska, S.; Vlatakis, I.; Mouchtaropoulou, E.; Siarkou, V. I.; Tychala, A.; Koutsioulis, D.; Skoura, L.; Argiriou, A.; Dovas, C. I., A one-step real-time RT-PCR assay for simultaneous typing of SARS-CoV-2 mutations associated with the E484K and N501Y spike protein amino-acid substitutions. J. Virol. Methods 2021, 296, 114242.

S2. Barlev-Gross, M.; Weiss, S.; Paran, N.; Yahalom-Ronen, Y.; Israeli, O.; Nemet, I.; Kliker, L.; Zuckerman, N.; Glinert, I.; Noy-Porat, T.; Alcalay, R.; Rosenfeld, R.; Levy, H.; Mazor, O.; Mandelboim, M.; Mendelson, E.; Beth-Din, A.; Israely, T.; Mechaly, A., Sensitive Immunodetection of Severe Acute Respiratory Syndrome Coronavirus 2 Variants of Concern 501Y.V2 and 501Y.V1. J. Infect. Dis. 2021, 224 (4), 616-619.

S3. Wang, Y.; Zhang, Y.; Chen, J.; Wang, M.; Zhang, T.; Luo, W.; Li, Y.; Wu, Y.; Zeng, B.; Zhang, K.; Deng, R.; Li, W., Detection of SARS-CoV-2 and Its Mutated Variants via CRISPR-Cas13-Based Transcription Amplification. Anal. Chem. 2021, 93 (7), 3393-3402.

S4. de Puig, H.; Lee, R. A.; Najjar, D.; Tan, X.; Soeknsen, L. R.; Angenent-Mari, N. M.; Donghia, N. M.; Weckman, N. E.; Ory, A.; Ng, C. F.; Nguyen, P. Q.; Mao, A. S.; Ferrante, T. C.; Lansberry, G.; Sallum, H.; Niemi, J.; Collins, J. J., Minimally instrumented SHERLOCK (miSHERLOCK) for CRISPR-based point-of-care diagnosis of SARS-CoV-2 and emerging variants. Sci. Adv. 2021, 7 (32).

S5. Kumar, M.; Gulati, S.; Ansari, A. H.; Phutela, R.; Acharya, S.; Azhar, M.; Murthy, J.; Kathpalia, P.; Kanakan, A.; Maurya, R.; Vasudevan, J. S.; S, A.; Pandey, R.; Maiti, S.; Chakraborty, D., FnCas9-based CRISPR diagnostic for rapid and accurate detection of major SARS-CoV-2 variants on a paper strip. Elife 2021, 10.